Experimental determination of band offsets at the SnS/CdS and SnS/InS_xO_y heterojunctions

A. M. Abdel Haleem[a] and M. Ichimura
Department of Engineering Physics, Electronics and Mechanics, Nagoya Institute of Technology, Gokiso, Showa, Nagoya 466-8555, Japan

(Received 28 October 2009; accepted 15 December 2009; published online 12 February 2010)

The semidirect x-ray photoelectron spectroscopy technique was used to measure the band alignments at the interface of heterostructures based on SnS. The layers were deposited by electrochemical deposition (ECD), chemical bath deposition (CBD), or photochemical deposition (PCD). The following four kinds of heterojunctions were characterized. (1) ECD-SnS/PCD-CdS. (2) CBD-SnS/PCD-CdS. (3) ECD-SnS/ECD-InS_xO_y. (4) CBD-SnS/ECD-InS_xO_y. The valence band offsets ΔE_V of those four heterojunctions are determined to be 1.34, 1.59, 0.77, and 0.74 ± 0.3 eV, respectively. © *2010 American Institute of Physics*. [doi:10.1063/1.3294619]

I. INTRODUCTION

The band offsets strongly affect the electrical transport properties of the heterojunction solar cell. The difference in the bandgap across the interface is distributed between a valance-band offset ΔE_V and a conduction-band offset ΔE_C. These offsets may form barriers for the charge carriers crossing the interface and dramatically influence the conversion efficiency of the heterojunction solar cell. Accordingly, for analyzing the solar cell performance, the study of its energy band diagram is essential.

Tin sulfide is a IV-VI compound semiconductor with layered orthorhombic structure. SnS thin films have been deposited by various techniques including simple techniques such as chemical bath deposition (CBD) and electrochemical deposition (ECD), and the band gap was reported to be 1.3–1.5 eV for the direct transition and 1.0–1.1 eV for the indirect transition.[1–9] It exhibits *p*-type conductivity and has a high absorption coefficient ($\alpha > 10^4$ cm^{-1}) comparable to that of CdTe in the visible range. Both Sn and S are nontoxic and abundant in nature. Thus SnS is a material of great interest in photovoltaic application.[10–13] We also reported fabrication of the SnS/InS_xO_y and SnS/CdS heterojunction solar cells.[14,15] Although their conversion efficiencies were low, they showed a rectifying property and photovoltaic effects.

There are two methods based on photoelectron spectroscopy which can be used to estimate the energy band structure of a certain heterojunction,[10] namely the direct and semidirect techniques. In the direct technique, the valence-band photoelectron spectra for the under layer surface and for the increasing upper layer surface are measured. At intermediate coverage (1.5–3 nm), both valence band leading edges are visible and a direct measurement of ΔE_V is possible by linear extrapolation of the two edges. This method is simple but cannot be applied to all interfaces. On the other hand, the semidirect technique, which is based on the measurement of core levels at the heterostructure interface and separate measurements of the valence band position with respect to the core levels for each constituent material, can be applied to all interfaces.[16–19] The semidirect technique allows the study of interfaces obtained by even simple deposition techniques like electrochemical or CBD techniques.[11] Actually, the semidirect method based on x-ray photoelectron spectroscopy (XPS) has been used to estimate the band alignment at the CdTe/CdS,[13,20] GaAs/AlAs,[21] β-In_2S_3/SnO_2,[22] $CuInSe_2/CdS$,[23] Cu_2S/CdS,[24] and AlN/Si interfaces.[25] This technique is used in the present study to estimate the energy band diagram of SnS/CdS and SnS/InS_xO_y heterojunctions. To our best knowledge, this is the first paper reporting an experimental estimation for the band offsets of SnS-based heterostructures.

II. EXPERIMENTAL PROCEDURE

A. Thin film preparation

Indium tin oxide (ITO)-coated glass sheets with dimensions equal to 1×1 cm^2 and sheet resistance about 8–9 Ω/sq were used as substrates in the present experiments. Before deposition, the substrates were cleaned ultrasonically in organic solvent (alkyl benzene) for 5 min and then dried by a steam of nitrogen gas. After deposition, films were left to dry in open air.

1. CdS

The CdS thin film was deposited onto ITO-coated glass substrates at room temperature by the photochemical deposition (PCD) technique from an aqueous solution containing 2 mmol/l $CdSO_4$ and 100 mmol/l $Na_2S_2O_3$.[14] The *p*H of the solution was adjusted to 3 by using diluted H_2SO_4. The substrate was fixed at 2 mm beneath the solution surface. The substrate was irradiated with a super high-pressure mercury arc lamp through a convergence lens focusing to about 10 mm diameter on the surface of the substrate, where the CdS layer was deposited. Deposition time was 30 min, and the thickness was around 0.1 μm. The film was annealed in nitrogen atmosphere for an hour at 100 °C.[14,26] The energy gap of the prepared sample equals $E_g^{CdS} = 2.4$ eV.

[a]Electronic addresses: cgt16503@stn.nitech.ac.jp and ashraf_ahaleem@yahoo.com.

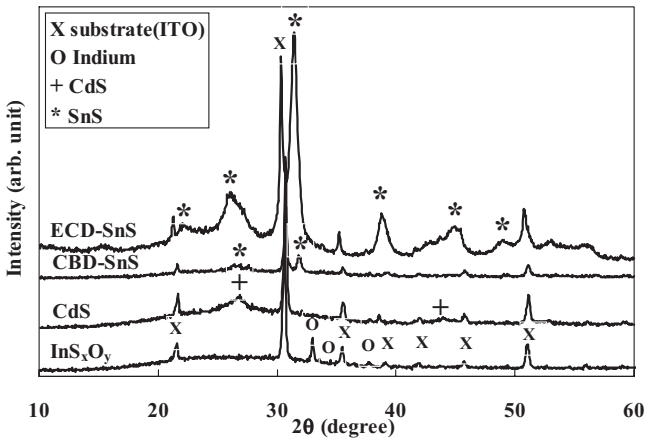

FIG. 1. XRD spectra for the individually prepared ECD-SnS, CBD-SnS, PCD-CdS, and ECD-InS_xO_y thin films.

2. SnS

The SnS thin films were deposited by ECD and CBD as follows.[27–29]

(A) ECD-SnS deposition conditions: the film was deposited using three-step pulse voltage (V1=0 V, V2=−1 V, V3=−0.6 V, and T1=T2=T3=10 s) from an aqueous bath containing 30 mmol/l $SnSO_4$ and 100 mmol/l $Na_2S_2O_3$ at room temperature.

(B) CBD-SnS deposition conditions: two aqueous bathes were used for deposition; the first bath contained $(NH_4)_2S_x$ (25 mmol/l) at room temperature and the second bath contained $SnCl_2$ (25 mmol/l) at 80 °C with *p*H=12.5 (adjusted by adding adequate amount of NaOH). The substrate was immersed sequentially in each bath for 5 s and the process was repeated until the required thickness was reached. (200 times is enough to deposit a 1 μm thick film).

The experimentally determined energy gap of the SnS sample prepared by ECD or CBD equals $E_g^{SnS}=1.3$ eV.

3. InS_xO_y

The indium sulfide oxide thin film was deposited by ECD using two-step pulse voltage (V1=−1.14 V, V2 =−0.4V, and T1=T2=10 s) from an aqueous solution containing 10 mmol/l $In_2(SO_4)_3$ and 100 mmol/l $Na_2S_2O_3$ at room temperature.[30] Postdeposition annealing was performed for the deposited film in nitrogen atmosphere for 1 h at 100 °C. The energy gap of the prepared sample equals $E_g^{InSO}=2.75$ eV.

B. Structural properties

The x-ray diffraction (XRD) measurements were carried out by the RIGAKU RINT-2000 diffractometer using Cu $K\alpha_1$ radiation for the individually prepared thin films. The measured ECD-SnS, CBD-SnS, PCD-CdS, and ECD-InS_xO_y thin films have thicknesses approximately equal to 2, 1.0, 0.1, and 0.2 μm, respectively. The XRD spectra, shown in Fig. 1, revealed that the ECD-SnS, CBD-SnS, and PCD-CdS have polycrystalline structures. However, the InS_xO_y thin film has an amorphous nature since no peaks related to indium compounds were observed. In addition, the film seems to include polycrystalline indium metal.

C. The XPS measurements

The semidirect method is explained taking SnS/CdS as an example. The XPS spectra were measured using the Al Kα line as an x-ray source. We first measured the Cd 4d and Sn 4d core levels $E_{Cd\ 4d}^{CdS}$ and $E_{Sn\ 4d}^{SnS}$ as well as the valence band maximum (VBM) E_V^{CdS} and E_V^{SnS} for CdS and SnS, respectively. These values were measured for the individual films deposited onto an ITO-coated glass substrate. The relative positions of the Cd 4d and Sn 4d core levels were then determined at the interface of the SnS/CdS heterostructure (bilayer). These last values were obtained from XPS spectra by the help of Ar^+ ion sputtering of the upper layer. The valence band offset ΔE_V at the heterojunction interface can be calculated as follows:

$$\Delta E_V^{SnS/CdS} = (E_{Sn\ 4d}^{SnS} - E_V^{SnS}) - (E_{Cd\ 4d}^{CdS} - E_V^{CdS}) - \Delta E_{CL}^{SnS/CdS}, \quad (1)$$

where $\Delta E_{CL}^{SnS/CdS}$ is the difference between Cd 4d and Sn 4d at the interface of SnS /CdS heterojunction. The conduction band discontinuities $\Delta E_C^{SnS/CdS}$ can then be calculated from

$$\Delta E_C^{SnS/CdS} = \Delta E_g^{SnS/CdS} - \Delta E_V^{SnS/CdS}, \quad (2)$$

where $\Delta E_g^{SnS/CdS}$ represents the difference in energy band gap between CdS and SnS thin films. The same method was applied to SnS/InS_xO_y heterostructure with the Cd 4d core level substituted by the In 4d core level in the above equations. The core level energy position was defined to be the center of the peak at half of the peak height, which made it unnecessary to resolve the spin orbit splitting of the relatively narrow Cd 4d, Sn 4d, and In 4d core levels.[19] The accuracy of the experimental measurement of the band offsets is limited primarily by the determination of the valence band edge from the experimental spectra. The top of the valence band was measured by linear extrapolation of the leading edge of the valence band XPS spectra. The accuracy of the XPS measurement in the present study is ±0.05 eV, therefore, the uncertainty of the band offset is ±0.3 eV.[16,22] Measurements were repeated on different samples to check their validity.

III. RESULTS AND DISCUSION

A. ECD-SnS/CdS

Figure 2(a) shows the XPS spectrum of the Cd 4d core level for the CdS thin film. The figure reveals that $E_{Cd\ 4d}^{CdS}$ =11.13 eV. Figure 2(b) shows the linear interpolation of the leading edge of the XPS spectrum measured for the CdS thin film. The figure reveals that $E_V^{CdS}=1.0$ eV. Figure 3(a) shows the XPS spectrum of the Sn 4d core level for the ECD-SnS thin film, which reveals that $E_{Sn\ 4d}^{SnS}=25.57$ eV. The linear interpolation of the leading edge of the spectrum measured for the ECD-SnS thin film reveals that $E_V^{SnS}=0.0$ eV as shown in Fig. 3(b). Figure 4 shows the XPS spectrum measured at the interface of the ECD-SnS/CdS heterojunction,

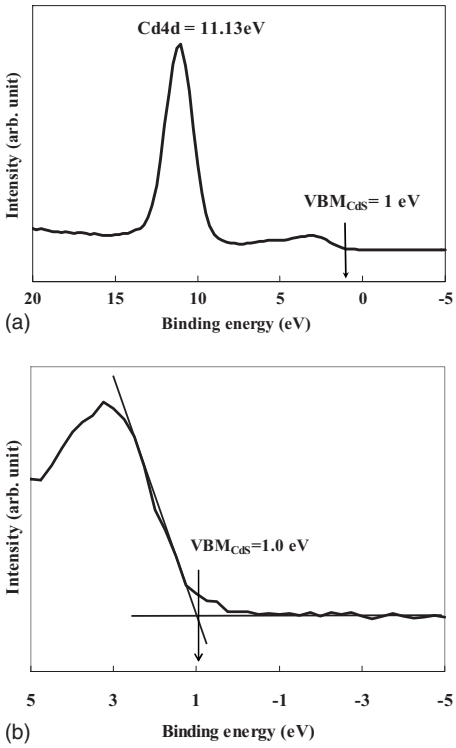

FIG. 2. (a) XPS spectrum of the Cd 4d core level measured at the bulk of the free-surface CdS thin film. (b) The linear interpolation of its leading edge.

where the Cd 4d and Sn 4d core levels equal 11.37 and 25.47 eV, respectively. This means that the difference between these core levels at the interface $\Delta E_{CL}^{ECD\text{-}SnS/CdS}=14.1$ eV. Consequently, by substituting those energy values in Eq. (1), the valence band offset $\Delta E_V^{ECD\text{-}SnS/CdS}$ at the heterojunction interface can be calculated as

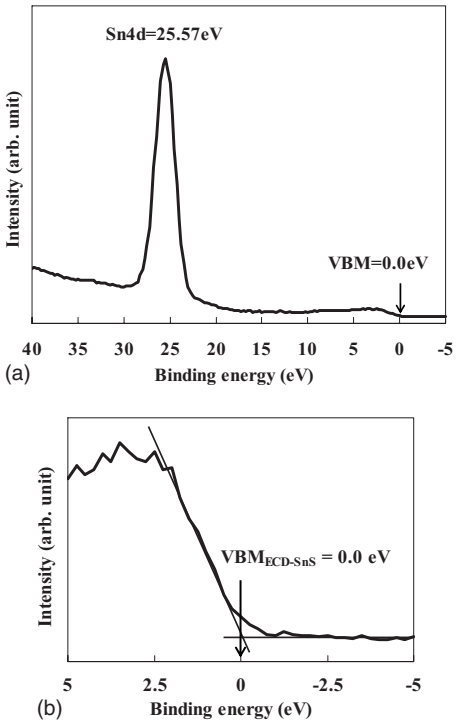

FIG. 3. (a) XPS spectrum of the Sn 4d core level measured at the bulk of the free-surface ECD-SnS thin film. (b) The linear interpolation of its leading edge.

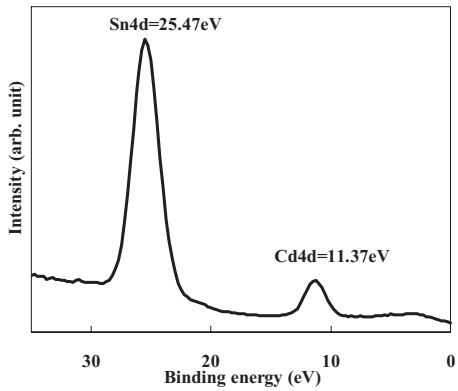

FIG. 4. Cd 4d and Sn 4d core levels measured at the interface of the ECD-SnS/CdS heterojunction.

$$\Delta E_V^{ECD\text{-}SnS/CdS} = (25.57 - 0.0) - (11.13 - 1.0) - 14.1 = 1.34 \text{ eV}. \quad (3)$$

Furthermore, the conduction band offset $\Delta E_C^{ECD\text{-}Sn/CdS}$ can be calculated by utilizing Eqs. (2) and (3) with the energy gap values of the CdS and SnS thin films:

$$\Delta E_C^{ECD\text{-}SnS/CdS} = \Delta E_g^{ECD\text{-}SnS/CdS} - \Delta E_V^{ECD\text{-}SnS/CdS} = (2.4 - 1.3) - 1.34 = -0.24 \text{ eV}. \quad (4)$$

The negative value means that the conduction band minimum (CBM) of CdS lies down that of SnS, as shown in Fig. 5. Thus, the junction at the ECD-SnS/CdS interface is of type II.

B. CBD-SnS/CdS

The Sn 4d core level ($E_{Sn\ 4d}^{CBD\text{-}SnS}$) and the VBM ($E_V^{CBD\text{-}SnS}$) measured at the bulk of the free-surface CBD-SnS thin film are 25.72 and 0.0 eV, respectively. The Sn 4d and Cd 4*d* core levels ($E_{Sn\ 4d}^{CBD\text{-}SnS}$ and $E_{Cd\ 4d}^{CdS}$) measured at the interface of the CBD-SnS/CdS heterojunction equal 25.5 and 11.5 eV, respectively. By substituting these energy values in Eqs. (1)

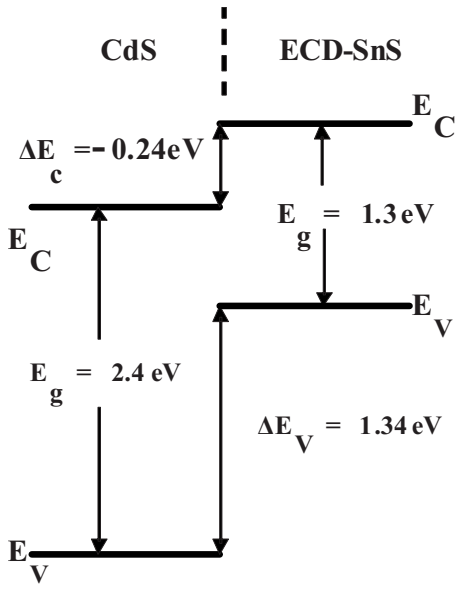

FIG. 5. Energy band diagram for the ECD-SnS/CdS heterojunction.

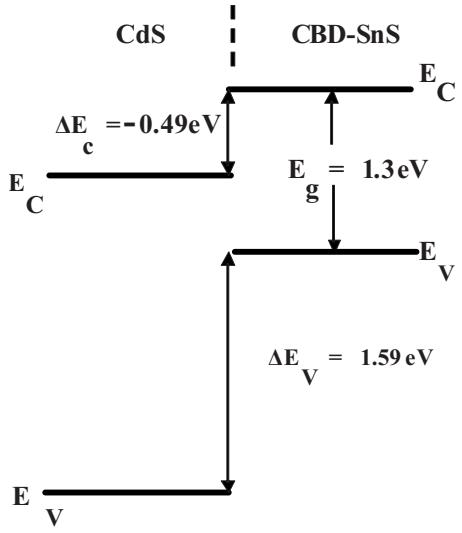

FIG. 6. Energy band diagram for the CBD-SnS/CdS heterojunction.

and (2), the valence and conduction band offsets at the interface of the CBD-SnS/CdS heterojunction are calculated as

$$\Delta E_V^{\text{CBD-SnS/CdS}} = 1.59 \text{ eV}, \quad (5)$$

$$\Delta E_C^{\text{CBD-SnS/CdS}} = -0.49 \text{ eV}. \quad (6)$$

The CBD-SnS/CdS heterojunction is of type II, as shown in Fig. 6. The comparison of Figs. 5 and 6 show that the location of the VBM and CBM of CBD-SnS are located at energy levels 0.25 eV higher than those of ECD-SnS when both are deposited onto CdS.

C. ECD-SnS/InS$_x$O$_y$

The XPS spectrum of the In 4d core level and the linear interpolation of the leading edge measured for the InS$_x$O$_y$ thin film reveal that $E_{\text{In 4d}}^{\text{InSO}}=18.25$ eV and $E_V^{\text{InSO}}=0.6$ eV, respectively. The In 4d and Sn 4d core levels measured at the interface of the ECD-SnS/InS$_x$O$_y$ heterojunction are equal to 18.26 and 25.41 eV, respectively. Consequently, the band offsets are calculated as

$$\Delta E_V^{\text{ECD-SnS/InSO}} = 0.77 \text{ eV}, \quad (7)$$

$$\Delta E_C^{\text{ECD-SnS/InSO}} = 0.68 \text{ eV}. \quad (8)$$

The estimated energy band diagram of the ECD-SnS/InS$_x$O$_y$ heterojunction is of type I, as shown in Fig. 7.

D. CBD-SnS/InS$_x$O$_y$

The In 4d and Sn 4d core levels ($E_{\text{In 4d}}^{\text{InSO}}$ and $E_{\text{Sn 4d}}^{\text{CBD-SnS}}$) measured at the interface of the CBD-SnS/InS$_x$O$_y$ heterojunction are equal to 18.01 and 25.34 eV, respectively. Consequently, the band offsets are calculated as

$$\Delta E_V^{\text{CBD-SnS/InSO}} = 0.74 \text{ eV}, \quad (9)$$

$$\Delta E_C^{\text{CBD-SnS/InSO}} = 0.71 \text{ eV}. \quad (10)$$

The estimated energy band diagram of the CBD-SnS/InS$_x$O$_y$ heterojunction is of type I, as shown in Fig. 8.

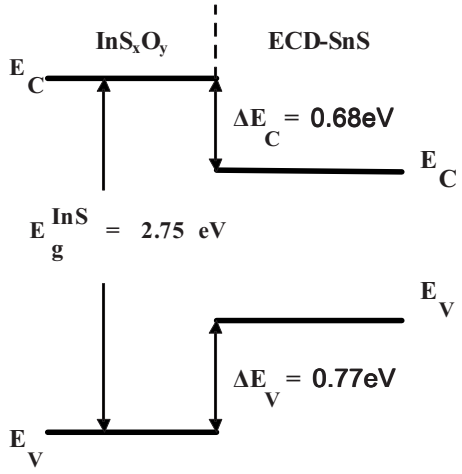

FIG. 7. Energy band diagram for the ECD-SnS/InS$_x$O$_y$ heterojunction.

The energy band diagrams drawn in Figs. 7 and 8 revealed that the VBM and CBM of CBD-SnS and ECD-SnS are located at almost the same energy levels with respect to those of InS$_x$O$_y$. Thus, the transitivity rule[31] does not hold for CBD-SnS and ECD-SnS in our experiment, i.e., the energy difference in VBM between CBD-SnS and ECD-SnS measured for SnS/InS$_x$O$_y$ is not the same as that measured for SnS/CdS.

As noted in Sec. III A, the InS$_x$O$_y$ films are amorphous, not crystalline. Differences in the photoelectron spectra between amorphous and crystalline phases have been investigated in detailed for In-based III-V materials.[32] The densities of the valence band states are remarkably different between the amorphous and crystalline phases, whereas the In 4d levels measured with respect to VBM are not significantly different between the phases. At present, it is not understood how much the amorphous nature of the InS$_x$O$_y$ films affects the measured band offset.

E. Consequences for solar cell properties

For a solar cell with n-type window layer and p-type absorber layer, the best photovoltaic output will be obtained when the conduction band offset is small and positive

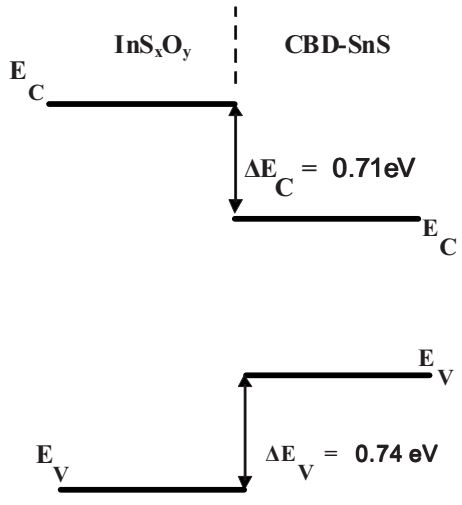

FIG. 8. Energy band diagram for the CBD-SnS/InS$_x$O$_y$ heterojunction.

$(0\ \text{eV} < \Delta E_C < 0.1\ \text{eV})$. If ΔE_C is negative, the open circuit voltage is limited by the built-in potential, which is smaller than the band gap of the absorber material by $-\Delta E_C$. A large positive ΔE_C will block the electron flow from the absorption layer to the window layer.

The preceding photoemission measurements of the SnS/CdS junctions indicated that both the CBM and the VBM at the interface were lower on the CdS side (i.e., a type II heterojunction). This type of junction implies unimpeded electron transport from the SnS side to the CdS side. However, a heterojunction of type II may suffer from recombination of the majority carriers at the interface resulting in decrease in the open circuit voltage and the cell conversion efficiency as well. This could partly explain the low conversion efficiency of the previously reported SnS/CdS-related solar cells.[5,6,14] In fact, reported values of open circuit voltage of SnS/CdS cells are generally low (0.2–0.35 V).

In case of the SnS/InS_xO_y heterojunctions, the measurements indicated that both the CBM and the VBM of the narrower energy gap material (SnS) at the interface lie in between those of the wider energy gap material (InS_xO_y) (type I heterojunction). The estimated value for the conduction band offset is relatively high ($\sim$0.7 eV) compared with that of the CdS/CIGS ($\sim$0.3 eV) and that of the CdS/CdTe (0.04 eV) heterojunctions.[23,13] Such a high spike at the conduction band acts as a barrier preventing the flow of the photogenerated electrons from the SnS side toward the InS_xO_y side. We fabricated SnS/InS_xO_y heterojunction cells by ECD,[26] which in fact showed a small short-circuit current. In addition, rectification properties were also poor and the open circuit voltage was very small. Therefore, for the ECD-SnS/InS_xO_y cells, the spike is not the only reason for the low efficiency.

Recently, the band offsets of SnS/CdS heterojunctions have been calculated on the basis of the density functional theory.[33] According to the calculation, SnS/CdS is a type I heterojunction, in contrast with the present experimental results. This discrepancy could be due to the fact that the rocksalt and zincblende structures were assumed for SnS in the calculation while the actual crystal structure of SnS is orthorhombic.

IV. CONCLUSION

In the present study, the band alignments at the interfaces of SnS/CdS and SnS/InS_xO_y heterostructures have been studied by the semidirect XPS technique. For ECD-SnS/CdS, CBD-SnS/CdS, ECD-SnS/InS_xO_y, and CBD-SnS/InS_xO_y interfaces, the valence band offsets are determined to be 1.34, 1.59, 0.77, and 0.74 ± 0.3 eV, respectively. The conduction band offsets for those heterostructures have also been calculated. The results show that the SnS/CdS heterojunctions are of type II while the SnS/InS_xO_y heterojunctions are of type I.

ACKNOWLEDGMENTS

We would like to thank Dr. M. Kato for his useful discussion and Mr. Moriguchi for his technical assistance. A. M. Abdel Haleem would like to thank the Egyptian government for supporting the present work.

[1] M. Parenteau and C. Carlone, Phys. Rev. B **41**, 5227 (1990).
[2] G. Valiukonis, D. A. Guseinova, G. Krivaite, and A. Sileika, Phys. Status Solidi B **135**, 299 (1986).
[3] K. Mishra, K. Rajeshwar, A. Weiss, M. Murley, R. D. Engelken, M. Slayton, and H. E. McCloud, J. Electrochem. Soc. **136**, 1915 (1989).
[4] M. T. S. Nair and P. K. Nair, Semicond. Sci. Technol. **6**, 132 (1991).
[5] H. Noguchi, A. Setiyadi, H. Tanamura, T. Nagatomo, and O. Omoto, Sol. Energy Mater. Sol. Cells **35**, 325 (1994).
[6] K. T. Ramakrishna Reddy, N. Koteswara Reddy, and R.W. Miles, Sol. Energy Mater. Sol. Cells **90**, 3041 (2006).
[7] K. Omoto, N. Fathy, and M. Ichimura, Jpn. J. Appl. Phys.,Part 1. **45**, 1500 (2006).
[8] M. Ichimura, K. Takeuchi, Y. Ono, and E. Arai, Thin Solid Films **361–362**, 98 (2000).
[9] D. Avellaneda, G. Delgado, M. T. S. Nair, and P. K. Nair, Thin Solid Films **515**, 5771 (2007).
[10] S. Chichibu, R. Sudo, N. Yoshida, Y. Harada, M. Uchida, S. Matsumoto, and H. Hugushi, Jpn. J. Appl. Phys., Part 2 **33**, L286 (1994).
[11] Y. Hashimoto, K. Taheuchi, and K. Ito, Appl. Phys. Lett. **67**, 980 (1995).
[12] A. D. Katnani and G. Margaritondo, Phys. Rev. B **28**, 1944 (1983).
[13] J. Fritsche, A. Thiben, A. Klein, and W. Jaegermann, Thin Solid Films **387**, 158 (2001).
[14] M. Gunasekaran and M. Ichimura, Sol. Energy Mater. Sol. Cells **91**, 774 (2007).
[15] A. M. Abdel Haleem and M. Ichimura, Jpn. J. Appl. Phys., Part 2 **48**, 035506 (2009).
[16] N. Barreau, S. Marsillac, J. C. Bernede, and L. Assmann, J. Appl. Phys. **93**, 5456 (2003).
[17] A. J. Nelson, J. Appl. Phys. **78**, 5701 (1995).
[18] D. A. Shirley, Phys. Rev. B **5**, 4709 (1972).
[19] E. A. Kraut, R. N. Grant, J. R. Waldrop, and S. P. Kowalczyk, Phys. Rev. Lett. **44**, 1620 (1980).
[20] J. Fritsche, D. Kraft, A. Thiben, T. Mayer, A. Klein, and W. Jaegermann, Thin Solid Films **403–404**, 252 (2002).
[21] J.R. Waldrop, S.P. Kowalczyk, R.W. Grant, E.A. Kraut, and L. Miller, J. Vac. Sci. Technol. **19**, 573 (1981).
[22] J. C. Bernède, N. Barreau, S. Marsillac, and L. Assmann Appl. Surf. Sci. **195**, 222 (2002).
[23] T. Schulmeyer, R. Hunger, A. Klein, W. Jaegermann, and S. Niki, Appl. Phys. Lett. **84**, 3067 (2004).
[24] G. Liu and T. Schulmeyer, J. Brötz, A. Klein, and W. Jaegemann, Thin Solid Films **431–432**, 477 (2003).
[25] H. Ishikawa, B. Zhang, T. Egawa, and T. Jimbo, Jpn. J. Physiol. **42**, 6413 (2003).
[26] A. M. Abdel Haleem and M. Ichimura, Thin Solid Films **516**, 7783 (2008).
[27] M. Ichimura and H. Takagi, Jpn. J. Appl. Phys. **47**, 7845 (2008).
[28] M. Ristov, Gj. Sinadinovski, I. Grozdanov, and M. Mitreski, Thin Solid Films **173**, 53 (1989).
[29] M. Ristov, G. Sinadinovski, M. Mitreski, and M. Ristova, Sol. Energy Mater. Sol. Cells **69**, 17 (2001).
[30] M. Ichimura, F. Goto, Y. Ono, and E. Arai, J. Cryst. Growth **198–199**, Part1, 308 (1999).
[31] A. D. Katnani and G. Margaritondo, J. Appl. Phys. **54**, 2522 (1983).
[32] J. N. J. Shevchik, J. Tejeda, and M. Cardona, Phys. Rev. B **9**, 2627 (1974).
[33] M. Ichimura, Sol. Energy Mater. Sol. Cells **93**, 375 (2009).